Author/s:
John Tokarsky, E;Crow, JC;Guenther, LM;Sherman, J;Taslim, C;Alexe, G;Pishas, KI;Rask, G;Justis, BS;Kasumova, A;Stegmaier, K;Lessnick, SL;Theisen, ER

Title:
Mitochondrial Dysfunction Is a Driver of SP-2509 Drug Resistance in Ewing Sarcoma

Date:
2022-07-01

Citation:
John Tokarsky, E., Crow, J. C., Guenther, L. M., Sherman, J., Taslim, C., Alexe, G., Pishas, K. I., Rask, G., Justis, B. S., Kasumova, A., Stegmaier, K., Lessnick, S. L. & Theisen, E. R. (2022). Mitochondrial Dysfunction Is a Driver of SP-2509 Drug Resistance in Ewing Sarcoma. Molecular Cancer Research, 20 (7), pp.1035-1046. https://doi.org/10.1158/1541-7786.MCR-22-0027.

Persistent Link:
https://hdl.handle.net/11343/320367

Mitochondrial Dysfunction Is a Driver of SP-2509 Drug Resistance in Ewing Sarcoma

E. John Tokarsky[1], Jesse C. Crow[1], Lillian M. Guenther[2], John Sherman[1], Cenny Taslim[1], Gabriela Alexe[2], Kathleen I. Pishas[3], Galen Rask[1], Blake S. Justis[1], Ana Kasumova[1], Kimberly Stegmaier[2], Stephen L. Lessnick[1,4], and Emily R. Theisen[1,4]

ABSTRACT

Expression of the fusion oncoprotein EWS/FLI causes Ewing sarcoma, an aggressive pediatric tumor characterized by widespread epigenetic deregulation. These epigenetic changes are targeted by novel lysine-specific demethylase-1 (LSD1) inhibitors, which are currently in early-phase clinical trials. Single-agent–targeted therapy often induces resistance, and successful clinical development requires knowledge of resistance mechanisms, enabling the design of effective combination strategies. Here, we used a genome-scale CRISPR–Cas9 loss-of-function screen to identify genes whose knockout (KO) conferred resistance to the LSD1 inhibitor SP-2509 in Ewing sarcoma cell lines. Multiple genes required for mitochondrial electron transport chain (ETC) complexes III and IV function were hits in our screen. We validated this finding using genetic and chemical approaches, including CRISPR KO, ETC inhibitors, and mitochondrial depletion. Further global transcriptional profiling revealed that altered complex III/IV function disrupted the oncogenic program mediated by EWS/FLI and LSD1 and blunted the transcriptomic response to SP-2509.

Implications: These findings demonstrate that mitochondrial dysfunction modulates SP-2509 efficacy and suggest that new therapeutic strategies combining LSD1 with agents that prevent mitochondrial dysfunction may benefit patients with this aggressive malignancy.

Introduction

Ewing sarcoma is the second most common bone malignancy in pediatric, adolescent, and young adult patients (1, 2). Five-year survival rates for patients with localized disease is 70% to 80%, but due to its highly aggressive nature, patients with metastatic, recurrent, or refractory tumors face poor outcomes with only 10% to 30% long-term survival (3, 4). Ewing sarcoma is histologically classified as a small, round, blue cell tumor, and has one of the lowest mutational burdens of any cancer (0.15 mutations/Mb; refs. 5–7). Ewing sarcoma is driven by a single fusion oncogene, most commonly EWS/FLI (2). EWS/FLI is the direct result of a *t*(11;22)(q24; q12) chromosomal translocation between the FET gene family member, Ewing sarcoma breakpoint region 1 protein (*EWSR1*), and the ETS transcription factor, Friend leukemia integration 1 transcription factor (*FLI1*). The resulting chimeric protein is a potent master transcriptional regulator and primary driver of oncogenesis (8, 9). EWS/FLI and other FET/ETS oncoproteins bind to DNA motifs containing either a consensus ETS motif (5′-*ACCGGAAGTG*-3′; refs. 10, 11) or microsatellites consisting of GGAA repeats (12). Binding to these DNA motifs allows EWS/FLI to promote chromatin accessibility and establish *de novo* enhancers (13). In addition, the low complexity domain of EWSR1 in EWS/FLI recruits chromatin regulators, such as BAF, NuRD, and p300 that are important for EWS/FLI-mediated activation and repression (14, 15).

Lysine-specific demethylase-1 (LSD1) is a flavin adenine dinucleotide–dependent amine oxidase that is highly expressed in Ewing sarcoma (16–18). LSD1 catalyzes the demethylation of mono- and di-methyl lysines at H3K4 and H3K9 (17) and is recruited by EWS/FLI as a member of the NuRD (19), and REST corepressor (CoREST; ref. 20) complexes. We have previously demonstrated that targeting LSD1 with the small-molecule inhibitor SP-2509 is efficacious in Ewing sarcoma preclinical models (21–23). SP-2509 is a reversible, allosteric inhibitor of LSD1 that halts Ewing sarcoma cell proliferation, induces apoptosis, and blocks tumor growth in preclinical Ewing sarcoma models (15, 18, 22). At present, an analog of SP-2509, known as seclidemstat (SP-2577, *Salarius Pharmaceuticals*), is currently in clinical trials to treat relapsed or refractory Ewing sarcoma (NCT03600649).

Acquired resistance to single-agent small molecules is a challenge in the development of novel cancer therapies. Given that small molecules targeting LSD1 could have an impact in patients with this aggressive disease, developing combination strategies to aid future clinical trials requires a deeper understanding of potential drug resistance pathways. Our laboratory previously generated an SP-2509–resistant Ewing sarcoma cell line from parental A673 cells through chronic exposure to escalating concentrations of SP-2509 (24). This resistant A673 cell line demonstrated a 55-fold greater IC_{50} value over parental A673 cells (7.5 vs. 0.18 μmol/L, respectively). Following removal of SP-2509 treatment, a 10-fold increased IC_{50} value (2 μmol/L) was maintained upon re-challenge, suggesting a non-reversible phenotype. No LSD1 mutations were identified in these cells, and instead a mutation in mitochondrial ribosomal protein L45 (*MRPL45*) was found in 85% of the drug-resistant cell population.

[1]Center for Childhood Cancer and Blood Diseases, Abigail Wexner Research Institute at Nationwide Children's Hospital, Columbus, Ohio. [2]Department of Pediatric Oncology, Dana-Farber Cancer Institute and Boston Children's Hospital, Harvard Medical School, Boston, Massachusetts. [3]Peter MacCallum Cancer Center, Melbourne, Victoria, Australia. [4]Department of Pediatrics, College of Medicine, The Ohio State University, Columbus, Ohio.

Note: Supplementary data for this article are available at Molecular Cancer Research Online (http://mcr.aacrjournals.org/).

Corresponding Author: Emily R. Theisen, Abigail Wexner Research Institute at Nationwide Children's Hospital, 700 Children's Drive, Columbus, OH 43205. Phone: 614-355-2927; E-mail: Emily.Theisen@NationwideChildrens.org

Mol Cancer Res 2022;20:1035–46

doi: 10.1158/1541-7786.MCR-22-0027

An emerging use for CRISPR screening technology is to determine genes whose deletion causes resistance to a drug of interest, thereby suggesting novel mechanisms involved in drug activity and potential escape pathways in cancer cells (25). We undertook a genome-scale CRISPR–Cas9 loss-of-function screen in two Ewing sarcoma cell lines in the presence of SP-2509. This identified genes involved in drug resistance related to mitochondrial function, specifically in the electron transport chain (ETC) complexes III (CIII) and IV (CIV). This was subsequently validated using genetic knockout (KO) models, ETC inhibitors, and mitochondrial depletion. SP-2509 treatment causes global changes in the transcriptome of Ewing sarcoma cells, and transcriptomic investigation of resistant cells using RNA-sequencing (RNA-seq) revealed that resistant cells show a blunted transcriptional response. We further report that the mitochondrial dysfunction that causes SP-2509 drug resistance also alters the transcriptional program enforced by EWS/FLI and LSD1. We propose that combining LSD1 inhibitors with agents that promote oxidative phosphorylation may be useful to circumvent these changes and prevent development of acquired resistance in Ewing sarcoma models.

Materials and Methods

Cell lines and reagents

Cell lines were sourced and cultured as described previously (12, 18, 26). A673 (ATCC Cat# CRL-1598, RRID: CVCL_0080) and SK-N-MC (ATCC Cat# CRL-2270, RRID: CVCL_1398) cell lines were obtained from the ATCC, TC-32 from Dr. Timothy Triche (Children's Hospital of Los Angeles, Los Angeles, CA), and SK-N-MC from Dr. Shu-Fang Jia (University of Texas, Houston, TX). Cell lines were validated yearly using STR profiling. Cell lines were tested for the presence of *Mycoplasma* using the Universal Mycoplasma testing kit every 3 to 4 months as needed and were most recently tested in December 2021. Cells that were freshly thawed were used up to two months in culture. Monoclonal cell lines generated in this study were expanded and stored long-term in 90% FBS and 10% DMSO in liquid nitrogen. Soft agar assays were performed as described previously (12, 18, 26). SP-2509 was purchased from Cayman Chemicals. Antimycin A, rotenone, and oligomycin were purchased from Thermo Fisher Scientific. All oligonucleotides used in this study were purchased from Integrate DNA Technologies, or Thermo-Fisher Scientific.

Genome-scale CRISPR–Cas9 KO screen

A genome-scale CRISPR–Cas9 KO screen was performed (Dana-Farber Cancer Institute, Boston, MA) using an Avana-4 lentiviral library with barcode sequences for sgRNAs located in Supplementary File S1. Ewing sarcoma cell lines, A673 and TC-32, cells were seeded and infected with the Avana-4 lentiviral library in 12-well tissue culture treated plates overnight before transfer to T-75 flasks. Cells were selected with puromycin and blasticidin for 6 to 7 days to ensure stable expression of Cas9 and sgRNA, respectively. Selection media were removed, and the cells recovered for 24 hours before treatment with either DMSO or 300 nmol/L SP-2509 ($n \geq 2$ for each condition). An early time point for each condition was collected, and the remaining cells were passaged for 2 weeks before the final collection. Genomic DNA was isolated, PCR amplified, and subjected to Illumina sequencing. The 5′ and 3′ PCR primers included the P5 (5′-AATGATACGGCGACCACCGA-3′) and P7 (5′-CAAGCAGAAGACGGCATACGAGAT-3′) Illumina adapter sequences. PoolQ (Broad Institute) was used to deconvolute samples by barcode and quantify the results.

Cloning and lentivirus production

All constructs used to target genes with CRISPR–Cas9 were produced by following the "Lentiviral CRISPR Toolbox" by Shalem and colleagues (27), with some minor modifications. To generate CRISPR–Cas9 constructs, a Control_sg plasmid containing the sgRNA under control of a U6 promoter and spCas9-NLS-1XFLAG-P2A-puro under the control of an EFS-NS promoter was used. Control_sg was digested with *BsmB1* and dephosphorylated overnight. The linear constructs were purified via agarose gel electrophoresis and QIAquick Gel Extraction Kit (Qiagen). Insert oligonucleotides were designed on the basis of the Avana-4 library single guide RNA (sgRNA) sequences (Supplementary Table S1; Supplementary File S1; ref. 27). Insert oligonucleotides were phosphorylated using T4 polynucleotide kinase (NEB) at 37°C for 1 hour and were annealed by heating to 95°C for 5 minutes and slowly cooled to room temperature. Annealed and phosphorylated oligonucleotides were diluted (1:200) and ligation reactions were performed at room temperature overnight and transformed into DH5α chemically competent *Escherichia coli*. Individual colonies were grown overnight, purified by Qiagen miniprep, and Sanger sequenced (Eurofins Scientific) to confirm insertion of desired sgRNA. Lentivirus was produced by transfecting EBNA (HEK-293) cells with 10 μg each of a CRISPR–Cas9 construct, LentiVSVG, and psPAX2 in OptiMEM and *Trans*IT-LT1 (Mirus). Transfected EBNA cells were incubated at 37°C for 48 hours, and virus was collected in modified DMEM. Virus was filtered (2 μm) and stored at −80°C.

CRISPR–Cas9 lentivirus transduction

A673 cells were seeded in 10-cm dishes (2×10^6 cells) and allowed to adhere overnight at 37°C. Cells were transduced by removing media and adding 2 mL of lentivirus and polybrene (10 μg/mL). Transduced plates were incubated at 37°C with gentle rocking every 30 minutes. After 2 hours, media (6 mL) containing polybrene (10 μg/mL) were added and the cells were left for 48 hours. Cells were selected with puromycin (2 μg/mL) were incubated for at least 48 hours, or until all cells on a control (non-transduced) plate were dead.

Generation of monoclonal cell lines

We generated long-term stable KOs of mitochondrial genes by performing lentiviral transduction in A673 cells (see above) and performing limited dilution in 96-well plates. After transduction and 2 days of selection, cells were serially diluted in A673 media containing puromycin. Cells were incubated at 37°C undisturbed for 1 week in 96-well plates. As single colonies reached confluency, they were transferred first to a 24-well plate and eventually to a 10-cm dish. These monoclonal cell lines were assayed via western blot to determine efficiency of gene KO, and subsequently assayed for cell proliferation and cell viability to assess drug resistance phenotype. Frozen aliquots of monoclonal populations were stored in 90% FBS and 10% DMSO and frozen in liquid nitrogen.

Western blot analysis

Antibodies for western blot analysis were sourced from either Thermo Fisher Scientific (MRPL45–PA5-54778, RRID: AB_2644155), Abcam (COA4–ab105678, RRID: AB_10860894; UQCRFS1–ab14746, RRID: AB_301445; CYC1, ab137757; NDUFS1–ab169540, RRID: AB_2687932; ATP5F1–ab84625, RRID: AB_1859955; SDHC–ab129736; Membrane Integrity WB Antibody Cocktail–ab110414, RRID: AB_2687585; FLI (EWS/FLI)–ab15289, RRID: AB_301825, or Cell Signaling Technology (LSD1–C69G12, RRID: AB_2070132). Dilutions of antibodies were performed on the basis of the manufacturer's protocol. Confirmation of gene KO was performed as

previously described (18). Densitometry values for western blot images were processed using ImageJ (NIH).

Cell viability assays

Cell viability was assessed by harvesting A673 cells or CRISPR/Cas9 modified cells and seeding in a 96-well white, opaque, tissue-culture treated plate (Corning) at a density of 5,000 to 8,000 cells per well in 200 μL of media. After adhering overnight, cells were treated with increasing concentrations of SP-2509 (50 μL, 0.01–30 μmol/L final concentration), or vehicle control (0.1% DMSO) for 72 hours, and each condition was repeated in triplicate. For ETC inhibitor studies, these inhibitors were added during the SP-2509 treatment step at a final concentration of 0.5 μmol/L for antimycin A and oligomycin A, and 0.05 μmol/L for rotenone. After 72 hours, 170 μL of media were removed from each well, and 80 μL of CellTiter-Glo (Promega) reagent was added to each well. Plates were agitated at 700 rpm for 2 minutes and allowed to incubate for 10 minutes shielded from ambient light. Luminescence was measured on a GloMax 96-well plate reader (Promega) and the cell viability was calculated relative to the vehicle treated wells. IC_{50} values were determined by using non-linear regression software GraphPad Prism 8.0 and fitting the data to log(SP-2509) versus response 4-parameter variable slope.

Statistical analysis

For cell viability assays, statistical analysis was performed by using GraphPad Prism 8.0. Comparing individual curve fits for logIC_{50} value was performed using an extra sum-of-squares F test. Compiled IC_{50} value data from multiple experiments were compared using the Student *t* test as indicated.

Seahorse XF assays

Metabolic flux analyses were performed using a Seahorse XFp flux analyzer (Agilent) following the manufacturer's protocols. Optimal cell seeding densities were determined for each cell line and condition. For mitochondrial stress tests, inhibitors (oligomycin, FCCP, rotenone/antimycin A) were prepared according to the manufacturer's protocol (Agilent). Data were analyzed using Agilent Wave software and GraphPad Prism.

RNA-seq analysis

Cells for RNA-Seq were prepared by seeding cells (1×10^6) on a 10-cm tissue culture treated plate and were incubated overnight at 37°C in 5% CO_2. Media were removed and replaced with media containing either 0.1% DMSO or 500 nmol/L SP-2509, each cell line and treatment condition had 2 replicates. After 48 hours of treatment with either DMSO or SP-2509, cells were harvested, and total mRNA was purified using the RNeasy kit (Qiagen) following the manufacturer's protocol, and on-column DNase digestion was performed. RNA was eluted from spin-columns using DEP-C–treated dH_2O, and RNA concentration was measured using QIAxpert (Qiagen). Duplicate RNA samples were submitted to the Institute for Genomic Medicine (IGM; Abigail Wexner Research Institute at Nationwide Children's Hospital, Columbus, OH) following IGM sample submission guidelines. Samples were sequenced using a Hi-Seq 4000 to generate 150 bp paired-end reads. STAR (2.7) was used to align reads to the human genome build hg19 and generate read counts for each gene. Genes with <1 count per sample were excluded from further analysis. DESeq2 was used for differential expression of gene counts. Volcano plots, principal component analysis (PCA), and heatmaps were generated in R. Heatmaps were generated using *pheatmap* with unsupervised hierarchical clustering. Scatterplots were generated using *ggplot2* and Pearson correlation coefficients were determined. Datasets were compared using gene set enrichment analysis (GSEA). Pathway comparison analysis was performed using compiled gene sets from our RNA-seq data and those accessible from MsigDB.

Software statement

All figures and schematics contained in this article were generated using Adobe Illustrator or as indicated in the Materials and Methods.

Results

A genome-scale CRISPR–Cas9 screen identifies unique mitochondrial gene deletions conferring SP-2509 resistance in Ewing sarcoma cells

Given the potential of LSD1 inhibitors for treating patients with Ewing sarcoma, we used an unbiased genomic screening approach to identify mechanisms of resistance to SP-2509. We performed a genome-scale CRISPR–Cas9 loss-of-function screen (**Fig. 1A**) using the Avana-4 lentiviral library (28, 29) that targets 18,333 human genes, with 74,378 sgRNAs, each carrying a unique barcode (Supplementary File S1). After transducing two SP-2509–sensitive cell lines, A673 and TC-32 (18), cells were treated with SP-2509 (300 nmol/L) or equivalent DMSO control, with the concentration optimized to promote positive selection of resistant cells. For each condition, cells were harvested at both an early time point (day 0) and at 14 days. Genomic DNA was then isolated from both treatment arms and barcodes were sequenced (**Fig. 1A**). The sgRNAs that provided a growth advantage with SP-2509 were enriched in the treated arm compared with DMSO controls. A core list of genes whose KO conferred resistance to SP-2509 was generated by examining z-scores calculated on sgRNA barcode reads by normalizing to an early time point. Using a $\log_2$ fold change ($\log_2$FC) expression of >2.5 and a significance value ($P < 0.05$) cutoff, we identified 245 and 176 genes in A673 and TC-32 cells, respectively, whose KO conferred SP-2509 resistance (**Fig. 1B**; Supplementary File S2).

Of these genes, 41 were common hits across both A673 and TC-32 cells (Supplementary Table S2). We analyzed these common genes for phenotypic signatures in the Molecular Signatures Database (MSigDB) that revealed mitochondrial metabolism, organelle organization and biogenesis, DNA damage/repair, and apoptosis pathways significantly enriched in the SP-2509–resistant state ($P < 0.05$; **Table 1**). Interestingly, 5 out of the top 10 most significantly enriched signatures were mitochondrial-related pathways (**Table 1**). The loss of genes encoding MRP, CIII and CIV proteins, and mitochondrial tRNA synthetases, but not mutations in ETC complexes I, II or V (CI, CII, CV), conferred SP-2509 resistance, suggesting specificity to particular pathways and not simply broad mitochondrial dysfunction (**Table 2**; **Fig. 1C**). Importantly, our CRISPR screen independently confirmed our previous finding of a stop-gain *MRPL45* mutation promoting acquired resistance to SP-2509 in A673 cells (24). In total, 74/78 possible MRPs and 18/56 possible mitochondrial tRNA synthetases (**Table 2**) were identified as positive hits in our CRISPR screen. MRPs and mitochondrial tRNA synthetases are required for translation of the human mitochondrial genome, which consists of 37 total genes that encode for 13 proteins, 22 tRNAs, and 2 rRNAs (30). The majority of the human mitochondrial genome encodes for proteins that form core subunits of ETC complexes I, III, IV, and V (31). Other nuclear-encoded genes that are important for replication, transcription, and translation of the mitochondrial genome were also found in our CRISPR screen (Supplementary File S2), including *POLG/G2* (polymerase gamma), and *POLRMT* (mitochondrial RNA polymerase).

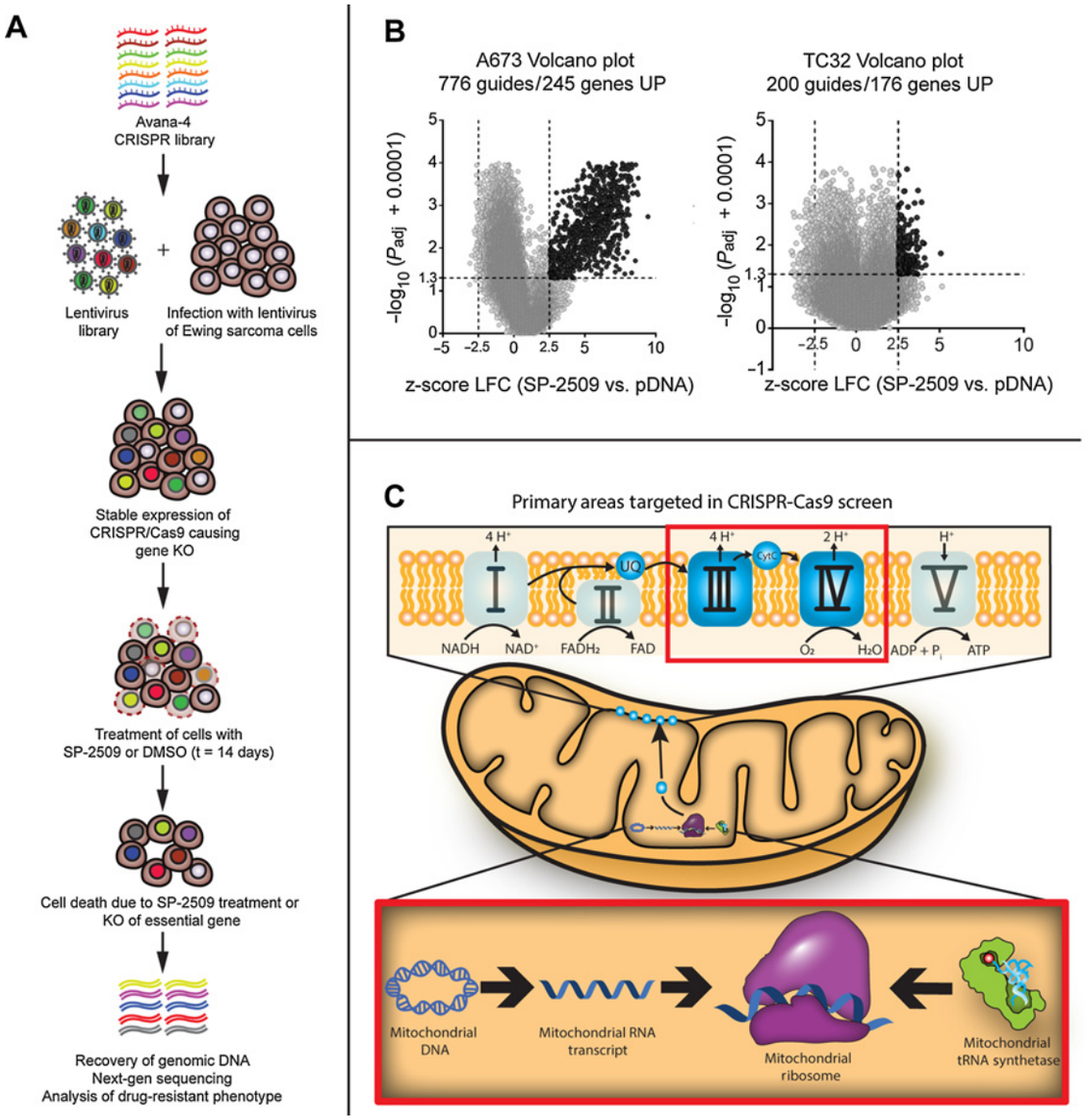

Figure 1.

CRISPR–Cas9 screen identifies mitochondrial dysfunction as a drug resistance phenotype. **A,** Overview of CRISPR–Cas9 screen. An Avana-4 library was used to generate a lentivirus library that was used to infect A673 and TC-32 cells that stably expressed Cas9. After antibiotic selection, cells were treated with either DMSO or 300 nmol/L SP-2509 for 14 days. Cells remaining after 14 days were collected, and their DNA was purified. PCR and barcoding were performed, followed by next-generation sequencing to identify the genes whose KO allowed cells to survive SP-2509 treatment. **B,** Volcano plots for A673 and TC-32 cells. Gene hits that had a $\log_2$Fold (LFC) z-score > 2.5, and a $-\log_{10} P_{adjusted}$ value of 0.05 (black dots) were considered significant. **C,** Representative images of the categories of mitochondrial genes that were identified in our CRISPR–Cas9 screen, including mitochondrial ribosomal proteins, mitochondrial tRNA synthetases, mitochondrial DNA-replication and transcription machinery, and ETC complexes III and IV. These components are surrounded by red boxes.

To validate this CRISPR screen, we generated KO of various genes of interest from the mitochondrial ribosome—*MRPL45*; CIII–Ubiquinol-Cytochrome C Reductase, Rieske Iron-Sulfur Polypeptide 1 (*UQCRFS1*) and cytochrome C1 (*CYC1*); and an CIV assembly factor–Cytochrome C Oxidase Assembly Factor 4 Homolog (*COA4*). We also generated KOs for CI–NADH:Ubiquinone Oxidoreductase Core Subunit S1 (*NDUFS1*), CII–Succinate Dehydrogenase C (*SDHC*), and CV–ATP synthase F(0) complex subunit B1 (*ATP5F1*). Cell viability assays were performed to test the efficacy of SP-2509 on these KO cells. We used sgRNA sequences identical to those found in the Avana-4 CRISPR library, and KO was confirmed by western blot (Supplementary Fig. S1). Mitochondrial hits from the CRISPR screen, including *MRPL45*, *UQCRFS1*, *CYC1*, and *COA4* either significantly increased the SP-2509 IC_{50} value or trended toward an increase in polyclonal KO populations (Supplementary Fig. S1). In contrast, polyclonal populations with sgRNAs targeting ETC components from CI (*NDUFS1*), CII (*SDHC*), and CV (*ATP5F1*) do not show any significant changes in SP-2509 IC_{50} (Supplementary Fig. S1). This preliminary validation effort confirmed

Table 1. Overlapping pathway analysis for A673 and TC-32 cell lines.

Index	Gene set type	OR	*P*
1	**MOOTHA_MITOCHONDRIA**	**4.6596**	**0.0032**
2	**ORGANELLE_ORGANIZATION_AND_BIOGENESIS**	**4.3913**	**0.0042**
3	**MOOTHA_HUMAN_MITODB_6_2002**	**3.9320**	**0.0127**
4	SPIELMAN_LYMPHOBLAST_EUROPEAN_VS_ASIAN_UP	3.5034	0.0196
5	RESPONSE_TO_STRESS	3.3007	0.0244
6	CELL_DEVELOPMENT	2.8859	0.0392
7	KEGG_HUNINGTONS_DISEASE	7.3313	0.0031
8	**WONG_MITOCHONDRIA_GENE_MODULE**	**6.2130**	**0.0054**
9	DNA_METABOLIC_PROCESS	5.2138	0.0097
10	**MOOTHA_PGC**	**3.1291**	**0.0479**

Note: Core 41 genes up from CRISPR/Cas9 screen versus MSigDB.
Bold text denotes pathways related to mitochondrial function.

the specificity of our CRISPR screen to particular components (MRPs, CIII, and CIV) of the mitochondria rather than general mitochondrial dysfunction.

Single-cell clones exhibiting KO of mitochondrial components show enhanced resistance to SP-2509

We found it notable that the specificity of hits enriching for CIII and CIV of the ETC, and the convergence with our prior studies (24), suggest that mitochondrial dysfunction is a *bona fide* driver of SP-2509 resistance. To better define the link between mitochondrial dysfunction and resistance to SP-2509, we isolated single cells following lentiviral transduction with CRISPR constructs, grew out monoclonal populations, and screened for clones containing complete gene loss (**Fig. 2A**). This method generated monoclonal cell populations containing KO of the following genes: *MRPL45* (MRPL45 KO); *UQCRFS1* (UQCRFS1 KO) and *CYC1* (CYC1 KO).

We first analyzed the impact of these gene KOs on mitochondrial function in our monoclonal populations using a seahorse instrument. This determined that both MRPL45 KO and CYC1 KO had significantly decreased basal respiration, whereas UQCRFS1 KO cells retained similar basal and maximal respiration to parental A673s (Supplementary Fig. S2). Cell viability assays indicated that each monoclonal KO cell line showed enhanced resistance to SP-2509 (**Fig. 2A**). This further confirmed the findings from the CRISPR screen and highlighted the ability of significantly reduced mitochondrial gene activity to dampen response to SP-2509.

ETC inhibitors targeting CIII, but not CI or CV, confer SP-2509 resistance in Ewing sarcoma cell lines

Having validated the CRISPR screen using genetic approaches, we next assayed whether loss of specific ETC complexes led to SP-2509 resistance using chemical probes targeting different complexes in the ETC. We used rotenone to block CI, antimycin A to block CIII, and oligomycin A to block CV. Initial optimization experiments identified 50 nmol/L rotenone, 500 nmol/L antimycin A, or 500 nmol/L oligomycin A as treatment conditions that could achieve sufficient ETC blockade during a 72-hour treatment (Supplementary Fig. S3). We then performed cell viability assays under dual treatment with SP-2509 (dose range, 0.01–30 μmol/L) and the various ETC inhibitors. We found that only antimycin A conferred drug resistance to SP-2509 compared with untreated cells in all 4 Ewing sarcoma cell lines tested (A673, TC-32, SK-N-MC, and TC-71; **Fig. 2B**). In contrast, neither CI nor CV inhibition significantly or consistently altered SP-2509 IC_{50} values (**Fig. 2B**). These results lend additional validation to the CRISPR screen findings, with chemical inhibition of the ETC at CIII, but not CI or CV, inducing resistance to SP-2509 in Ewing sarcoma cells.

Loss of mitochondria leads to resistance to SP-2509 in A673 cells

Genetic and chemical approaches validated our initial findings that specific components of the mitochondria, including mitochondrial transcriptional and translational machinery and ETC complexes CIII and CIV, are important for sensitivity to SP-2509, and loss of these components confers resistance. We therefore asked whether resistance arose following the loss of a specific mitochondrial function, or instead as a result of residual organelle dysfunction. To address this question, we depleted mitochondria from cells using mitophagy, generating mitochondrial null (mt_0) A673 cells. In this system, YFP-tagged Parkin (YFP-Parkin), an E3 ubiquitin ligase, is retrovirally transduced and mitochondrial stress is caused with the protonophore FCCP. YFP-Parkin localizes to the stressed mitochondria and induces

Table 2. CRISPR–Cas9 screen gene hits clustered on the basis of mitochondrial gene groups.

	Gene type	#Hits/gene type	Example gene
Positive hits in CRISPR screen	Mitochondrial ribosomal subunits	74/78	*MRPL45*
	Ubiquinol-Cytochrome c reductase (Complex III)	7/10	*UQCRFS1*
	Cytochrome C reductase (Complex IV)	8/19	*COX5A*
	Mitochondrial tRNA synthetases	18/56	*MARS2*
Negative hits in CRISPR screen	NADH:ubiquinone oxidoreductase (Complex I)	1/45	*NDUFS1*
	Succinate dehydrogenase (Complex II)	0/4	*SDHC*
	ATP Synthase (Complex V)	0/20	*ATP5F1*

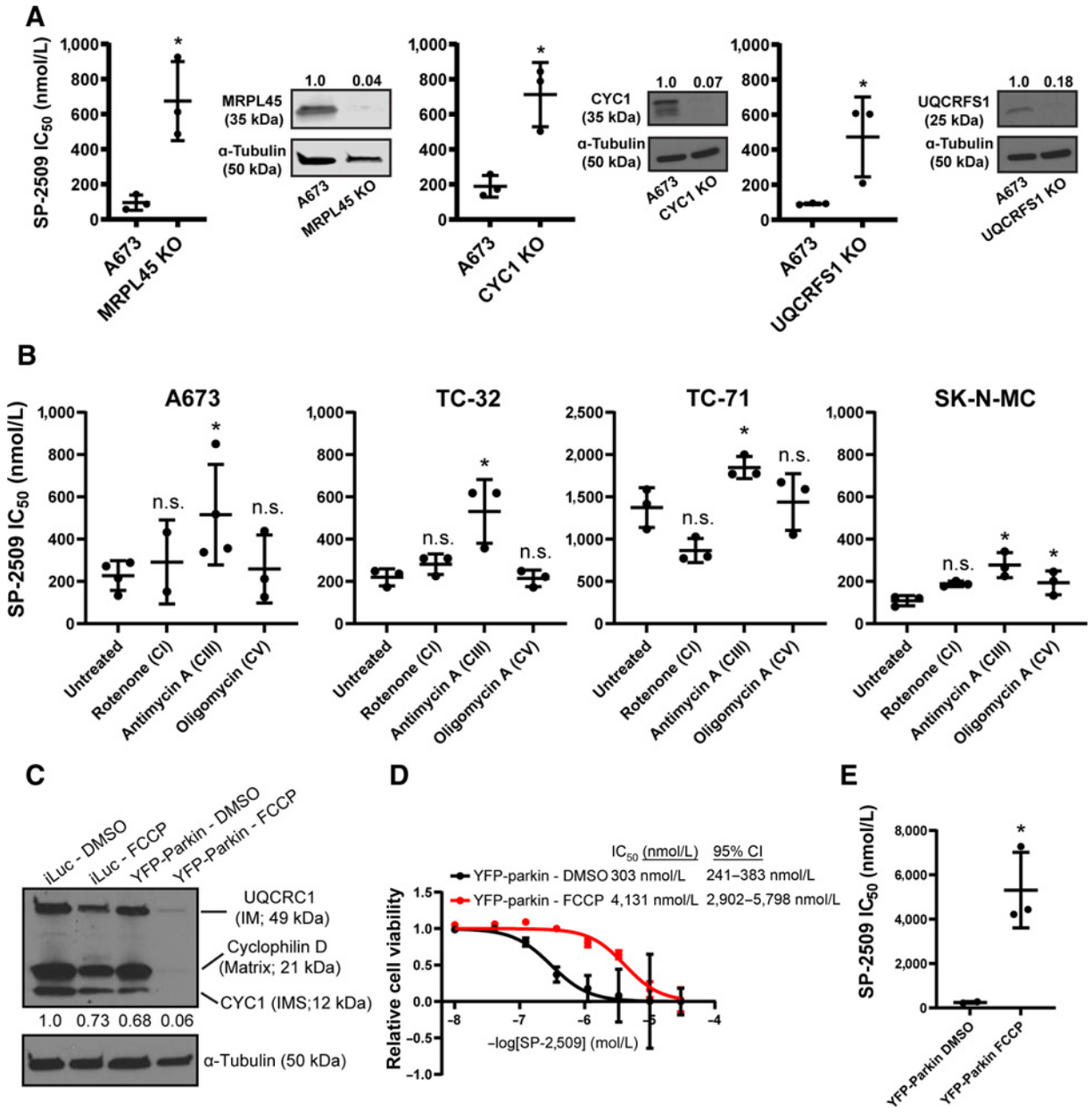

Figure 2.

Validation of CRISPR screen through genetic KO, chemical inhibition, and mitochondrial depletion. **A,** Compiled SP-2509 IC_{50} data and western blot images for monoclonal KO cells; mitochondrial ribosomal protein L45 (MRPL45 KO), Ubiquinone-Cytochrome C Reductase, Rieske Iron-Sulfur Polypeptide 1 (UQCRFS1 KO), Cytochrome C1 (CYC1 KO). Compiled data are from $n = 3$ independent experiments. Statistical analysis was performed by using a Student *t* test. Data that reached a significance *P* value of ≤0.05 are denoted with *. Densitometry values are indicated for each protein band and are quantified as previously described in the Materials and Methods. **B,** Compiled SP-2509 IC_{50} data for simultaneous treatment of indicated cell lines with SP-2509 and ETC inhibitors, rotenone (CI), antimycin A (CIII), or oligomycin (CV). Compiled data are from $n = 3$ independent experiments. Statistical analysis was performed by using a Student *t* test comparing each inhibitor treatment with the untreated cell lines, with * denoting a significance (*P* value) of ≤ 0.05, and values that are not significant denoted as n.s. **C,** Western blot analysis of $mt_{\varnothing}$ cells for mitochondrial proteins using Membrane Integrity WB Antibody Cocktail (Abcam; ab110414). Samples are denoted with A673 cells infected with retroviral constructs for YFP-Parkin and iLuc (mock infection), that were treated with either DMSO or FCCP for 48 hours. Blots for Ubiquinone–cytochrome c reductase core protein 1 (UQCRC1) represents the mitochondrial intermembrane (IM), Cyclophilin D in the mitochondrial matrix, cytochrome C1 (CYC1) in the mitochondrial intermembrane space (IMS), and α-tubulin was used as a loading control. Depletion of these proteins in the YFP-Parkin–FCCP condition indicates depletion of mitochondria from the cells. **D,** Dose–response curve comparing A673 cells expressing YFP-Parkin either treated with DMSO or FCCP. **E,** Compiled SP-2509 IC_{50} data for $mt_{\varnothing}$ cells. Compiled data are from $n = 3$ independent experiments. Statistical analysis was performed by using a Student *t* test comparing each inhibitor treatment with the untreated cell lines, with * denoting a significance (*P* value) of ≤ 0.05.

mitophagy (Supplementary Fig. S4A; ref. 32). We confirmed mitochondrial depletion via western blot with a mitochondrial antibody cocktail recognizing proteins in the inner-membrane, the inner-membrane space, and the mitochondrial matrix (**Fig. 2C**). Retroviral transduction with a mock control (iLuc) confirmed that FCCP alone did not deplete mitochondria (**Fig. 2C**) or promote resistance to SP-2509 (Supplementary Fig. S4B). We performed a Seahorse assay to confirm mt_{o} cells had lost their oxidative capacity (Supplementary Fig. S4C). Cell viability assays performed after SP-2509 treatment in our mt_{o} cells showed a mean IC_{50} value of 5,309 nmol/L, 21-fold higher than the mean IC_{50} value observed with control cells (mean $IC_{50} = 244$ nmol/L; $P = 0.02$; **Fig. 2D** and **E**). These data support that the loss of specific mitochondrial functions, rather than the resulting cellular dysfunction, contributes to SP-2509 resistance.

RNA-seq reveals KO clones show differing response to SP-2509

We have previously shown that LSD1 enforces EWS/FLI-mediated transcription and that SP-2509 treatment reverses EWS/FLI-mediated gene regulation (18, 33). Given that the functional relevance of mitochondrial status on LSD1 and EWS/FLI activity is unknown, and that mitochondrial dysfunction imparted resistance to SP-2509, we next tested whether resistant cells showed altered LSD1-EWS/FLI activity and how the transcriptional response to SP-2509 in resistant cells differed from sensitive cells. Following 48 hours of treatment with either vehicle or 500 nmol/L SP-2509, parental A673 cells, MRPL45 KO cells, CYC1 KO cells, and UQCRFS1 KO cells were assayed by RNA-seq and differentially expressed genes (DEG) were determined (**Fig. 3A**). As has been shown previously in A673 cells, SP-2509 treatment altered the expression of thousands of genes (12,125 total DEGs; 6,929 upregulated; and 5,196 downregulated). Interestingly, we saw differing transcriptional responses among our monoclonal cell lines. UQCRFS1 KO cells showed the greatest number of DEGs (11,528 total DEGs; 6,373 upregulated; and 5,155 downregulated), comparable with A673. Both CYC1 KO (7,351 total DEGs; 3,855 upregulated; and 3,496 downregulated) and MRPL45 KO cells showed fewer DEGs (4,681 DEGs total; 2,925 upregulated; and 1,756 downregulated) suggesting a blunted transcriptional response. PCA revealed that vehicle-treated CYC1 KO, UQCRFS1 KO, and A673 cells cluster together, whereas vehicle-treated MRPL45 KO cells cluster apart from this group along the first principal component (PC1) axis (**Fig. 3B**). SP-2509 treatment generally caused a shift along the principal component 2 (PC2) axis, with variable effects on each cell type. The largest shift was seen for parental A673 cells and UQCRFS1 KO cells, with lesser effects on CYC1 KO cells and an even further diminished response for MRPL45 KO cells. These effects agree with the total number of DEGs observed in each cell line and suggest a spectrum of transcriptional response, with the most resistant cells showing the smallest change in transcriptome, and vice versa.

Because we observed that all cell lines shifted in the same direction along PC2 to varying degrees following SP-2509 treatment, we next hypothesized that similar genes were changing in response to treatment. To address this, we used Venn analysis to compare the SP-2509–induced DEGs in A673 cells with those identified in the various monoclonal KO cell lines (**Fig. 3C**). We found that a majority of the DEGs in each KO cell line were shared with A673 cells (**Fig. 3C**). We noted that the more resistant cell lines had a smaller number of DEGs and a high degree of overlap between DEGs in KO lines and A673s. Therefore, we next asked whether decreased responsiveness arose because either a subset of genes failed to respond to treatment or that all genes decreased in their responsiveness resulting in a lower number of genes exceeding the cutoffs to define a DEG. To do this, we plotted the observed fold change for a given gene in a monoclonal KO cell line against the fold change observed for that gene in A673 cells, separating up- and downregulated genes (**Fig. 3D**). Significant correlation was observed between the transcriptional response in all KO cell lines with that in A673 cells (all $P < 2.2 \times 10^{-16}$), whereas the strength of the correlation, measured by both the R value and the slope of the line of best fit, varied across cell lines. As suggested by the number of DEGs, PCA analysis, and the Venn analysis, UQCRFS1 KO showed the strongest correlation in both upregulated and downregulated genes ($R = 0.81$ slope $= 0.83$ and $R = 0.62$ slope $= 0.56$, respectively). This was then followed by CYC1 KO (upregulated: $R = 0.64$, slope $= 0.41$; downregulated: $R = 0.42$, slope $= 0.23$), whereas MRPL45 KO showed the weakest correlation (upregulated: $R = 0.51$, slope $= 0.17$; downregulated: $R = 0.30$, slope $= 0.12$). This demonstrates that as you move from least resistant (UQCRFS1 KO) to more resistant (CYC1 KO) to most resistant (MRPL45 KO); the transcriptional response to SP-2509 is globally diminished, akin to turning down the "volume" of this response. Together, these data show that though SP-2509 largely regulates the same genes in A673 cells and mitochondrial KO lines, altering the mitochondrial function in A673s blunts the response to SP-2509.

Mitochondrial dysfunction induces transcriptional changes that mimic SP-2509 treatment

We reasoned that the observed decrease in transcriptional response to SP-2509 could arise either because the genes regulated by SP-2509 were more resistant to change or because KO of mitochondrial genes had already altered expression of these genes. To further distinguish between these possibilities, we first identified the basal transcriptional changes induced by KO in all three monoclonal cell lines. This revealed that MRPL45 KO had the greatest DEGs with respect to A637 cells (12,098 total DEGs; 6,163 upregulated; and 5,935 downregulated), followed by CYC1 KO (8,026 total DEGs; 4,632 upregulated; and 3,384 downregulated), and then UQCRFS1 KO (6,868 total DEGs; 3,434 upregulated; and 3,434 downregulated), in agreement with the PCA in **Fig. 3B** (Supplementary Table S3). Interestingly, the number of DEGs observed in the most resistant MRPL45 KO cells was comparable with that observed for SP-2509–treated A673 cells. We then used GSEA (34) to investigate whether the DEGs caused by mitochondrial dysfunction were functionally related to those DEGs caused by SP-2509 treatment in A673 cells. Using |normalized enrichment score (NES)| > 1.5 as a cutoff value for significance, GSEA revealed that upregulated and downregulated genes in MRPL45 KO cells (NES: 2.9 and −3.6, respectively) shared significant functional similarity with SP-2509 treatment in A673 cells (**Fig. 4A**). Both UQCRFS1 KO (upregulated NES: 1.5; downregulated NES: −2.9) and CYC1 KO (upregulated NES: 1.7; downregulated NES: −2.9) displayed functional similarity to SP-2509 treatment, albeit with lower NESs when upregulated genes were analyzed (**Fig. 4B**; Supplementary Fig. S5). These data indicate that our monoclonal KO cell lines have undergone significant transcriptional changes that resemble treatment with SP-2509, supporting a model wherein the transcriptional response to SP-2509 is diminished in resistant cells because the transcriptome already resembles that of a treated cell.

Taken together, our transcriptomic data suggest that our most resistant MRPL45 KO cells displayed a basal transcriptome that most resembled SP-2509 treatment and had the weakest transcriptional response to SP-2509 treatment, and vice versa with our least resistant UQCRFS1 KO cells. We next hypothesized that the combination of basal transcriptional changes induced by mitochondrial dysfunction along with further transcriptional changes induced by SP-2509

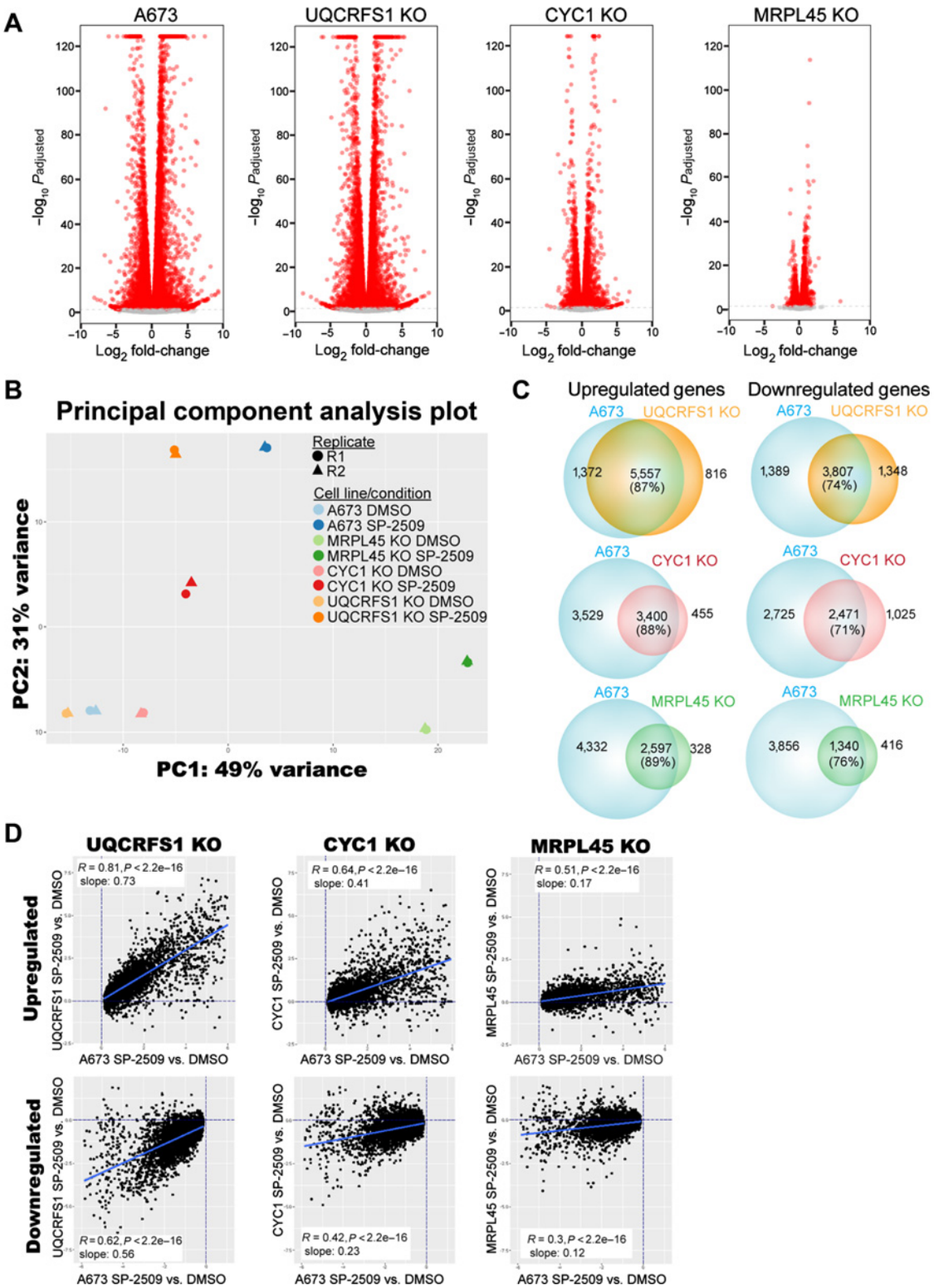

Figure 3.

RNA-seq of monoclonal mitochondrial KO cell lines. **A,** Volcano plots comparing SP-2509 treatment versus DMSO treatment for each indicated cell line. Each dot represents a differentially expressed gene (DEG) with significantly changed DEGs (red) having a $-\log_{10} P_{adjusted} < 0.05$, and non-significant DEGs (gray) failing to reach significance. (*Continued on the following page.*)

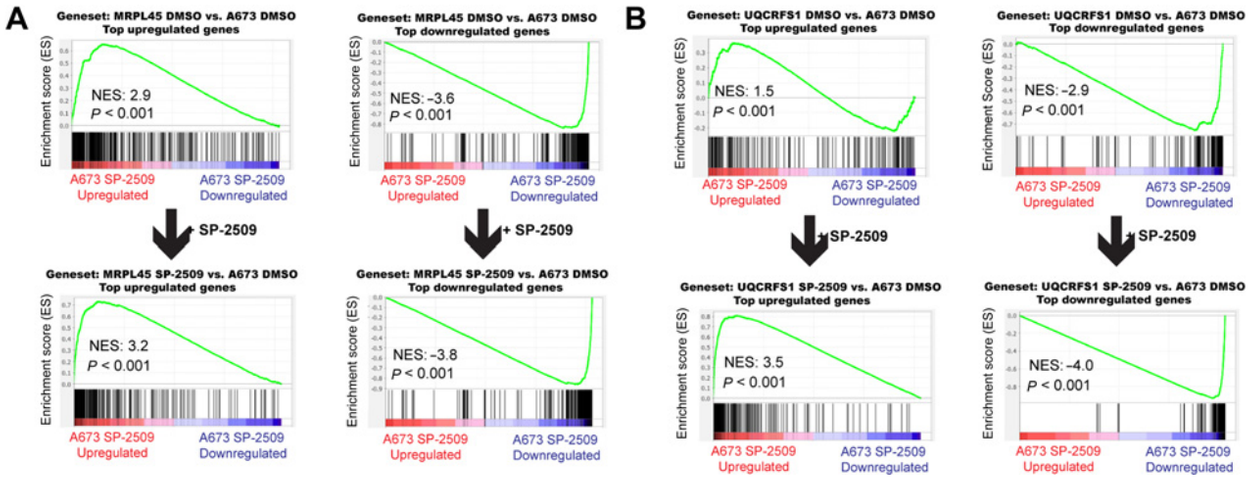

Figure 4.

Gene set enrichment analysis (GSEA) of monoclonal KO cell lines compared with SP-2509–treated A673 cells. GSEA from RNA-seq experiments using differentially expressed genes (DEG) for A673 cells treated with SP-2509 (A673 SP-2509 vs. A673 DMSO) as the rank-ordered list (ROL). The ROL was used for each comparison with a geneset for MRPL45 KO (**A**) and UQCRFS1 KO (**B**) of the top upregulated and downregulated genes. The top represents comparisons for the 480 most upregulated and downregulated genes for the indicated monoclonal KO treated with DMSO versus A673 DMSO. The bottom represents GSEA for the most upregulated and downregulated genes for the indicated monoclonal KO treated with SP-2509 versus A673 DMSO. Arrows indicate changes in gene expression from DMSO treated cells to SP-2509–treated cells. Normalized enrichment scores (NES) and *P* values are shown for each GSEA.

treatment would more completely recapitulate the SP-2509 transcriptional signature of sensitive A673 cells. To address this question, we used GSEA to compare the DEGs from monoclonal KO cells treated with SP-2509 with respect to parental A673 cells to the A673 SP-2509 transcriptional signature. Interestingly, for our MRPL45 KO cells treated with SP-2509 (**Fig. 4A**; bottom), there was no substantial change in NES scores for upregulated genes (NES: 2.9 → 3.2) or downregulated genes (NES: −3.6 → −3.8). This analysis supports that the MRPL45 KO basal transcriptional profile largely resembled an A673 cell treated with SP-2509 and is consistent with the observation that MRPL45 KO cells have the most blunted response to SP-2509 treatment. In contrast, UQCRFS1 KO cells (**Fig. 4B**; bottom) showed an increased functional enrichment for both upregulated (NES: 1.5 → 3.5) and downregulated (NES: −2.9 → −3.9) genes. Similar results were obtained for CYC1 KO cells (Supplementary Fig. S5; upregulated genes—NES: 1.7 → 3.1; downregulated genes—NES: −2.9 → −3.8). These analyses demonstrate that transcriptional regulation due to KO of mitochondrial genes resembles SP-2509 treatment to varying degrees generally correlating with the level of resistance. Less resistant cells CYC1 KO and UQCRFS1 KO cells show further transcriptional changes in response to SP-2509 treatment.

Because the transcriptome of our monoclonal KO cell lines resembled an A673 cell treated with SP-2509 and because SP-2509 reverses EWS/FLI transcriptional activity, we next hypothesized that mitochondrial dysfunction also disrupted EWS/FLI transcriptional activity (18, 22). We used GSEA to compare the transcriptional changes associated with our mitochondrial KO lines with the EWS/FLI transcriptional signature. This revealed that EWS/FLI transcriptional activity is decreased in both MRPL45 KO (upregulated NES: −2.8; downregulated NES: 2.3), and CYC1 KO (upregulated NES: −2.2; downregulated NES: 1.9) (Supplementary Fig. S6). In contrast, UQCRFS1 KO results in upregulation of a subset of EWS/FLI-repressed genes (upregulated NES: −2.0) but has limited impact in blunting EWS/FLI-mediated gene activation (downregulated NES: −2.1). Because LSD1 and EWS/FLI regulate similar targets, we expanded this analysis to LSD1-mediated gene regulation (Pishas and colleagues, ref. 18). Compared with EWS/FLI-mediated transcriptional activity, LSD1-mediated transcriptional activity was more affected by mitochondrial dysfunction in MRPL45 KO cells (upregulated NES: −4.1; downregulated NES: 3.8) and CYC1 KO cells (upregulated NES: −3.1; downregulated NES: 2.0). Again, in contrast, UQCRFS1 KO demonstrated no reversal of the LSD1 transcriptional activity (upregulated NES: 1.9; downregulated NES: −3.7). Together, these data indicate that both EWS/FLI and LSD1 require mitochondrial activity in Ewing sarcoma cells, and that mitochondrial dysfunction disrupts EWS/FLI- and LSD1-mediated gene regulation. This disruption may explain a reduction in oncogenic potential observed in MRPL45 KO and CYC1 KO cells, but not UQCRFS1 KO cells (Supplementary Fig. S7). Notably, though both EWS/FLI (22) and LSD1 depletions confer resistance to SP-2509 treatment (Supplementary Fig. S8A–S8C), and we show that EWS/FLI and LSD1 protein levels are stable across the KO cell

(*Continued.*) **B,** Principal component analysis (PCA) plot of the transcriptional profiles of indicated monoclonal KO cell lines and parental A673 cells. Principal component 2 (PC2) on the *y*-axis is plotted against principal component 1 (PC1) on the *x*-axis. Different cell conditions are depicted by color and replicates are represented with different shapes. **C,** Venn diagrams comparing the overlap of differentially expressed genes caused by treatment with SP-2509 for A673 versus the indicated monoclonal KO cell line. **D,** Scatterplots depicting common genes differentially regulated during treatment with SP-2509 for parental A673 cells versus each indicated monoclonal KO cell line. Data are plotted as $\log_2$FC of each monoclonal KO cell on the *y*-axis against the $\log_2$FC of A673 parental cells on the *x*-axis. Dotted lines depict $x = 0$ and $y = 0$. Significance was defined as Benjamini–Hochberg $P_{adjusted} < 0.05$ with no fold-change cutoff values. Lines of best fit were derived from the linear model only for genes with significant changes in both parental and monoclonal KO cells to represent the common DEGs. Pearson correlation coefficients and their *P* values are depicted with the slope from the linear model in the boxed inset.

lines tested here (Supplementary Fig. S8D and S8E). This suggests that alternative mechanisms may link mitochondrial function to transcriptional regulation in Ewing sarcoma cells and this is an important area for future studies.

Discussion

Effective targeted therapies are urgently needed to treat recurrent or refractory Ewing sarcoma, and a promising clinical molecule, seclidemstat, may help these patients. Unfortunately, clinical use is often hindered by intrinsic- or acquired-drug resistance that renders targeted therapeutics ineffective (35, 36). Identifying and understanding potential drug resistance pathways will aid in the development of combinational therapies that suppress resistance, or screening approaches to identify the patients with greatest potential for benefit. As we have addressed in this report and previously (24), drug resistance arising through mitochondrial dysfunction may hinder efficacy in patients with Ewing sarcoma. In this study, we demonstrate through genomic screening and validate using genetic and chemical approaches, that SP-2509 drug resistance is mediated by mitochondrial dysfunction in Ewing sarcoma. We further demonstrate that mitochondrial dysfunction causes transcriptional changes in Ewing sarcoma that mimic EWS/FLI and LSD1 depletion and thus blunts the cellular response to SP-2509.

In this study, a short-term dosing strategy was used to identify mutations in mitochondrial proteins that may cause drug resistance to LSD1 inhibitors. An inherent limitation to this approach is that these results may neither reflect rates of mutation in a patient tumor microenvironment, nor the length of time needed to develop mutations in mitochondrial genes. However, in our prior work generating resistance using a long-term dosing strategy, we found the predominant driver of resistance to also be an *MRPL45* mutation. This suggests that our approach here further validates and builds upon our previous findings.

Mitochondria act as the key metabolic hub for the cell by producing ATP and other macromolecule precursors that aid in cell proliferation. In addition, many studies have shown that mitochondria act as a key signaling hub and interact with the nucleus by generating metabolites important for chromatin regulation, a process known as retrograde signaling (37–39). For example, a subset of gastrointestinal stromal tumors is caused by mutations in succinate dehydrogenase (CII) enzymes, resulting in an accumulation of succinate that leads to inhibition of ten–eleven translocation (TET) dioxygenases and dysregulation of histone demethylation (40, 41). Mitochondrial metabolites such as acetyl-CoA, succinate, fumarate, α-ketoglutarate (α-KG), S-adenosyl methionine (SAM) and the oncometabolite, L-2-HG, are all responsible for regulating chromatin modifying enzymes such as histone acetylases, histone demethylases such as Jumonji C domain-containing proteins, and DNA demethylases such as TET dioxygenases (37, 42). Changes in the mitochondrial ETC proteins also can have profound effects on the function of cells. For example, regulatory T cells with CIII deficiency led mice to develop systemic inflammation, thymic atrophy, enlargement of lymph nodes, significantly activated $CD4^+$ and $CD8^+$ T cells, and impaired viability past 3 weeks of age (43). The CIII-deficient regulatory T cells had an increase in DNA hypermethylation and gene expression changes via the buildup of 2-HG and succinate, and a decreased ratio of NAD^+/NADH (43). Currently, it is unclear how mitochondria in Ewing

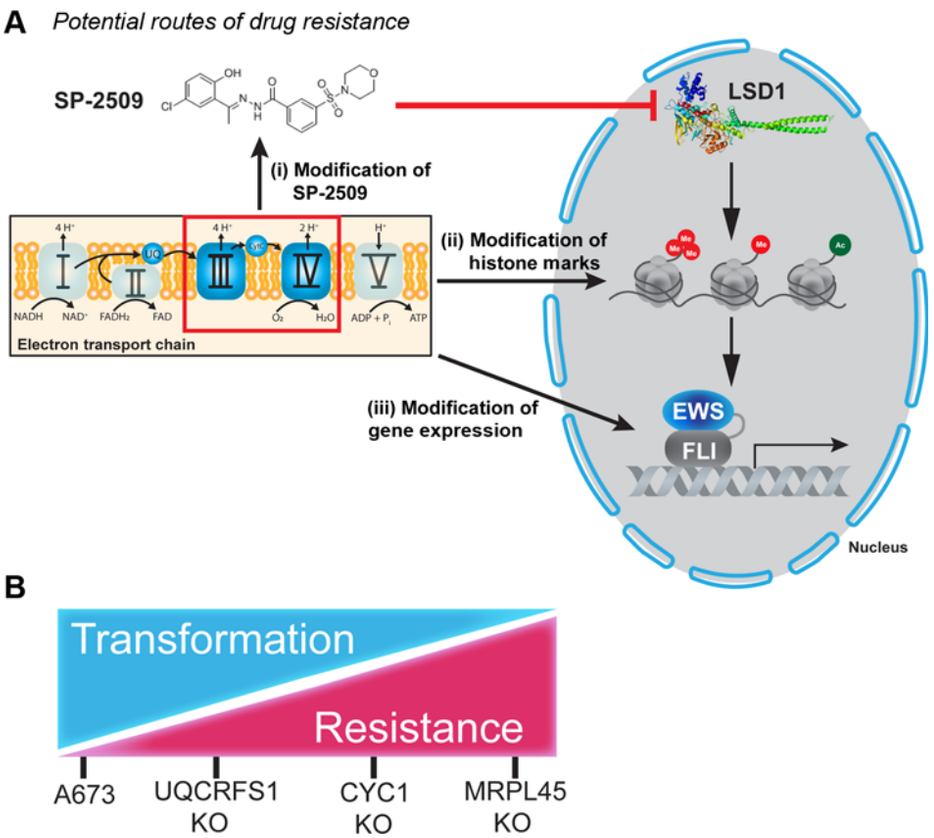

Figure 5.
Model for mitochondrial influence on SP-2509 drug resistance and oncogenic transformation ability in Ewing sarcoma. **A,** Each arrow indicates a potential route for the mitochondrial ETC to influence SP-2509 treatment of Ewing sarcoma. **B,** Transformation/SP-2509 drug resistance model for mitochondrial dysfunction in Ewing sarcoma with A673 and each monoclonal cell line indicated.

sarcoma are involved in altering chromatin and transcriptional regulation through LSD1, or otherwise. In this study, we observed large changes in basal gene expression for our monoclonal KO cell lines, indicating that transcriptional regulation is dramatically altered by mitochondrial dysfunction (**Fig. 3**; Supplementary Table S3). Furthermore, this differential regulation of gene expression in our monoclonal KO cells appears to blunt the response to SP-2509 in Ewing sarcoma cells.

Though this study examines potential routes of SP-2509 resistance in Ewing sarcoma, the mechanism by which drug resistance arises is not fully understood. In **Fig. 5A**, we propose a preliminary model with each arrow representing a distinct (but not exclusive) situation where mitochondria could potentially influence SP-2509 treatment. First, mitochondria containing functional CIII and CIV could directly activate SP-2509, through chemical modification, and this activated SP-2509 could be required to inhibit LSD1. Second, as has been shown in other studies (37, 42–44), mitochondrial metabolites could play a role in changing the epigenetic marks on histones. This could potentially alter the function and/or localization of LSD1 (or other enzymes) on chromatin, thus influencing the epigenetic landscape of the cell and this potential mechanism is the subject of ongoing studies. Finally, mitochondria may be influencing the basal gene expression of each cell, which is a phenomenon we observed with our monoclonal cells (**Figs. 3** and **4**). Adopting a transcriptome that resembles an SP-2509–treated cell likely requires the engagement of compensatory mechanisms to prevent cell death. In addition, an unknown off-target specificity of SP-2509 that directly targets a component of mitochondrial function may exists that is unrelated to LSD1 inhibition. Though this is not an exhaustive list of potential drug resistance mechanisms, our work here allows us to address each of these potential pathways in future studies.

This study has defined mitochondrial dysfunction as a *bona fide* mechanism of drug resistance in Ewing sarcoma. Here, we have shown that loss of specific complexes of the mitochondria, particularly ETC CIII and CIV, causes resistance to SP-2509. However, these proteins are essential for proper cellular function, and we showed that disruption of mitochondrial protein function also alters oncogenic transformation (Supplementary Fig. S7). Thus, a trade-off may occur in Ewing sarcoma cells that have mitochondrial dysfunction, whereby they gain the ability to resist SP-2509/seclidemstat treatment but lose their ability to survive and proliferate in a tumor microenvironment (**Fig. 5B**). This spectrum of transformation/drug resistance is exemplified by our monoclonal KO cells with our most resistant cell line MRPL45 KO, unable to undergo oncogenic transformation, whereas our least resistant cell line UQCRFS1 KO retains the ability to undergo oncogenic transformation. CYC1 KO cells are moderately resistant to SP-2509, and still retain some ability to undergo oncogenic transformation. Therefore, these data offer valuable insights into potential combination therapeutics that may promote dependence on mitochondrial metabolism, in particular oxidative phosphorylation, to promote more long-term efficacy of LSD1 inhibitors. Potential combination approaches may be achieved by using mitochondrial modulators such as BH3 mimetics (obatoclax and navitoclax) or the oxidative stress inducing compound, Elesclomol. The BH3 mimetics, obatoclax and navitoclax, are compounds that drive the intrinsic apoptosis pathway and have been shown to be effective at targeting Ewing sarcoma (45). Elesclomol has been shown to promote apoptosis in Ewing sarcoma cells by leading to elevated ROS, particularly in mitochondrial ROS (46).

Ongoing and future clinical trials involving LSD1 inhibitors, such as SP-2577, may benefit from incorporating biological correlates that assess mitochondrial function. Furthermore, these data may be useful for clinicians using RNA-seq of patient biopsies to look for an SP-2509–like gene signature before treatment. This would indicate that the tumor would likely be less responsive to LSD1 inhibition. Alternatively, whole-exome sequencing could be used to screen for patients that may have potential mitochondrial mutations or mutations in genes that are known to affect mitochondrial function.

Authors' Disclosures

E.J. Tokarsky reports grants from CancerFree KIDS during the conduct of the study. J. Sherman reports grants from CancerFree KIDS outside the submitted work. K.I. Pishas reports grants from Alex's Lemonade Stand (Young Investigator Grant) and NHMRC (CJ Martin, Overseas Biomedical Fellowship) during the conduct of the study. K. Stegmaier reports grants from National Cancer Institute and St Baldrick's Foundation during the conduct of the study; as well as personal fees from AstraZeneca, other support from Bristol Myers Squibb, grants from Novartis, personal fees from Auron Therapeutics, and grants and personal fees from KronosBio outside the submitted work. S.L. Lessnick reports personal fees from Salarius Pharmaceuticals outside the submitted work; as well as a patent for "Methods and compositions for the diagnosis and treatment of Ewing's sarcoma" issued and "Diagnosis and treatment of drug-resistant Ewing's sarcoma" issued; and served on the scientific advisory board for Salarius Pharmaceuticals. E.R. Theisen reports other support from Salarius Pharmaceuticals and grants from CancerFree KIDS outside the submitted work. No disclosures were reported by the other authors.

Authors' Contributions

E.J. Tokarsky: Formal analysis, validation, investigation, visualization, methodology, writing–original draft, writing–review and editing. **J.C. Crow:** Formal analysis, investigation, methodology, writing–review and editing. **L.M. Guenther:** Conceptualization, formal analysis, investigation, methodology, writing–review and editing. **J. Sherman:** Formal analysis, investigation, methodology, writing–review and editing. **C. Taslim:** Data curation, software, formal analysis, writing–review and editing. **G. Alexe:** Data curation, software, formal analysis, writing–review and editing. **K.I. Pishas:** Conceptualization, funding acquisition, writing–review and editing. **G. Rask:** Formal analysis, investigation, writing–review and editing. **B.S. Justis:** Formal analysis, investigation, writing–review and editing. **A. Kasumova:** Formal analysis, investigation, writing–review and editing. **K. Stegmaier:** Conceptualization, funding acquisition, writing–review and editing. **S.L. Lessnick:** Conceptualization, resources, supervision, funding acquisition, visualization, methodology, project administration, writing–review and editing. **E.R. Theisen:** Resources, data curation, software, formal analysis, supervision, funding acquisition, validation, visualization, methodology, project administration, writing–review and editing.

Acknowledgments

We acknowledge funding from SLL and ERT startup fund (40306-0011 and 40306-0025), Hyundai Hope on Wheels (810665-1222-00), and CancerFree KIDS (810752-1222-00). NIH R35 CA210030 and St. Baldrick's Foundation Robert J. Arceci Innovation Award (to K. Stegmaier). K.I. Pishas acknowledges financial support from the University of Adelaide Florey Medical Research Foundation Clinical Cancer Research Fellowship, NHMRC CJ Martin Overseas Biomedical Fellowship (APP1111032), and the Alex's Lemonade Stand Young Investigators Grant (APP37138). L.M. Guenther is a William Raveis Charitable Fund Physician–Scientist of the Damon Runyon Cancer Research Foundation (PST-20-18) and acknowledges support from the Rally Foundation for Childhood Cancer Research. We would like to thank Ariunaa Bayanjargal, Megann Boone, Andrea Byrum, Julia Selich-Anderson, and Iftekhar Showpnil for helpful discussion and careful editing of this article.

The costs of publication of this article were defrayed in part by the payment of page charges. This article must therefore be hereby marked *advertisement* in accordance with 18 U.S.C. Section 1734 solely to indicate this fact.

Received January 11, 2022; revised February 23, 2022; accepted March 14, 2022; published first March 17, 2022.

References

1. Burningham Z, Hashibe M, Spector L, Schiffman JD. The epidemiology of sarcoma. Clin Sarcoma Res 2012;2:14.
2. Delattre O, Zucman J, Plougastel B, Desmaze C, Melot T, Peter M, et al. Gene fusion with an ETS DNA-binding domain caused by chromosome translocation in human tumours. Nature 1992;359:162–5.
3. Grunewald TGP, Cidre-Aranaz F, Surdez D, Tomazou EM, de Alava E, Kovar H, et al. Ewing sarcoma. Nat Rev Dis Primers 2018;4:5.
4. Gaspar N, Hawkins DS, Dirksen U, Lewis IJ, Ferrari S, Le Deley MC, et al. Ewing sarcoma: current management and future approaches through collaboration. J Clin Oncol 2015;33:3036–46.
5. Brohl AS, Solomon DA, Chang W, Wang J, Song Y, Sindiri S, et al. The genomic landscape of the Ewing sarcoma family of tumors reveals recurrent STAG2 mutation. PLoS Genet 2014;10:e1004475.
6. Crompton BD, Stewart C, Taylor-Weiner A, Alexe G, Kurek KC, Calicchio ML, et al. The genomic landscape of pediatric Ewing sarcoma. Cancer Discov 2014;4: 1326–41.
7. Lawrence MS, Stojanov P, Polak P, Kryukov GV, Cibulskis K, Sivachenko A, et al. Mutational heterogeneity in cancer and the search for new cancer-associated genes. Nature 2013;499:214–8.
8. Turc-Carel C, Philip I, Berger MP, Philip T, Lenoir GM. Chromosome study of Ewing's sarcoma (ES) cell lines. Consistency of a reciprocal translocation t(11;22) (q24;q12). Cancer Genet Cytogenet 1984;12:1–19.
9. Turc-Carel C, Aurias A, Mugneret F, Lizard S, Sidaner I, Volk C, et al. Chromosomes in Ewing's sarcoma. I. An evaluation of 85 cases of remarkable consistency of t(11;22)(q24;q12). Cancer Genet Cytogenet 1988;32:229–38.
10. Wei GH, Badis G, Berger MF, Kivioja T, Palin K, Enge M, et al. Genome-wide analysis of ETS-family DNA-binding in vitro and in vivo. EMBO J 2010;29: 2147–60.
11. Szymczyna BR, Arrowsmith CH. DNA binding specificity studies of four ETS proteins support an indirect read-out mechanism of protein-DNA recognition. J Biol Chem 2000;275:28363–70.
12. Johnson KM, Mahler NR, Saund RS, Theisen ER, Taslim C, Callender NW, et al. Role for the EWS domain of EWS/FLI in binding GGAA-microsatellites required for Ewing sarcoma anchorage independent growth. Proc Natl Acad Sci U S A 2017;114:9870–5.
13. Riggi N, Knoechel B, Gillespie SM, Rheinbay E, Boulay G, Suva ML, et al. EWS-FLI1 utilizes divergent chromatin remodeling mechanisms to directly activate or repress enhancer elements in Ewing sarcoma. Cancer Cell 2014; 26:668–81.
14. Boulay G, Sandoval GJ, Riggi N, Iyer S, Buisson R, Naigles B, et al. Cancer-specific retargeting of BAF complexes by a prion-like domain. Cell 2017;171:163–78.
15. Sankar S, Bell R, Stephens B, Zhuo R, Sharma S, Bearss DJ, et al. Mechanism and relevance of EWS/FLI-mediated transcriptional repression in Ewing sarcoma. Oncogene 2013;32:5089–100.
16. Bennani-Baiti IM, Machado I, Llombart-Bosch A, Kovar H. Lysine-specific demethylase 1 (LSD1/KDM1A/AOF2/BHC110) is expressed and is an epigenetic drug target in chondrosarcoma, Ewing's sarcoma, osteosarcoma, and rhabdomyosarcoma. Hum Pathol 2012;43:1300–7.
17. Shi Y, Lan F, Matson C, Mulligan P, Whetstine JR, Cole PA, et al. Histone demethylation mediated by the nuclear amine oxidase homolog LSD1. Cell 2004; 119:941–53.
18. Pishas KI, Drenberg CD, Taslim C, Theisen ER, Johnson KM, Saund RS, et al. Therapeutic targeting of KDM1A/LSD1 in Ewing sarcoma with SP-2509 engages the endoplasmic reticulum stress response. Mol Cancer Ther 2018;17:1902–16.
19. Wang Y, Zhang H, Chen Y, Sun Y, Yang F, Yu W, et al. LSD1 is a subunit of the NuRD complex and targets the metastasis programs in breast cancer. Cell 2009; 138:660–72.
20. Chen Y, Yang Y, Wang F, Wan K, Yamane K, Zhang Y, et al. Crystal structure of human histone lysine-specific demethylase 1 (LSD1). Proc Natl Acad Sci U S A 2006;103:13956–61.
21. Theisen ER, Pishas KI, Saund RS, Lessnick SL. Therapeutic opportunities in Ewing sarcoma: EWS-FLI inhibition via LSD1 targeting. Oncotarget 2016;7: 17616–30.
22. Sankar S, Theisen ER, Bearss J, Mulvihill T, Hoffman LM, Sorna V, et al. Reversible LSD1 inhibition interferes with global EWS/ETS transcriptional activity and impedes Ewing sarcoma tumor growth. Clin Cancer Res 2014;20: 4584–97.
23. Sorna V, Theisen ER, Stephens B, Warner SL, Bearss DJ, Vankayalapati H, et al. High-throughput virtual screening identifies novel N'-(1-phenylethylidene)-benzohydrazides as potent, specific, and reversible LSD1 inhibitors. J Med Chem 2013;56:9496–508.
24. Pishas KI, Lessnick SL. Ewing sarcoma resistance to SP-2509 is not mediated through KDM1A/LSD1 mutation. Oncotarget 2018;9:36413–29.
25. Sulahian R, Kwon JJ, Walsh KH, Pailler E, Bosse TL, Thaker M, et al. Synthetic lethal interaction of SHOC2 depletion with MEK inhibition in RAS-driven cancers. Cell Rep 2019;29:118–34.
26. Theisen ER, Miller KR, Showpnil IA, Taslim C, Pishas KI, Lessnick SL. Transcriptomic analysis functionally maps the intrinsically disordered domain of EWS/FLI and reveals novel transcriptional dependencies for oncogenesis. Genes Cancer 2019;10:21–38.
27. Shalem O, Sanjana NE, Hartenian E, Shi X, Scott DA, Mikkelson T, et al. Genome-scale CRISPR–Cas9 knockout screening in human cells. Science 2014; 343:84–7.
28. Meyers RM, Bryan JG, McFarland JM, Weir BA, Sizemore AE, Xu H, et al. Computational correction of copy-number effect improves specificity of CRISPR–Cas9 essentiality screens in cancer cells. Nat Genet 2017;49:1779–84.
29. Doench JG, Fusi N, Sullender M, Hegde M, Vaimberg EW, Donovan KF, et al. Optimized sgRNA design to maximize activity and minimize off-target effects of CRISPR–Cas9. Nat Biotechnol 2016;34:184–91.
30. Taanman JW. The mitochondrial genome: structure, transcription, translation, and replication. Biochim Biophys Acta 1999;1410:103–23.
31. Gammage PA, Frezza C. Mitochondrial DNA: the overlooked oncogenome? BMC Biol 2019;17:53.
32. Correia-Melo C, Ichim G, Tait SW, Passos JF. Depletion of mitochondria in mammalian cells through enforced mitophagy. Nat Protoc 2017;12:183–94.
33. Theisen ER, Selich-Anderson J, Miller KR, Tanner JM, Taslim C, Pishas KI, et al. Chromatin profiling reveals relocalization of lysine-specific demethylase 1 by an oncogenic fusion protein. Epigenetics 2021;16:405–24.
34. Subramanian A, Tamayo P, Mootha VK, Mukherjee S, Ebert BL, Gillette MA, et al. Gene set enrichment analysis: a knowledge-based approach for interpreting genome-wide expression profiles. Proc Natl Acad Sci U S A 2005;102:15545–50.
35. Groenendijk FH, Bernards R. Drug resistance to targeted therapies: deja vu all over again. Mol Oncol 2014;8:1067–83.
36. Sarmento-Ribeiro AB, Scorilas A, Goncalves AC, Efferth T, Trougakos IP. The emergence of drug resistance to targeted cancer therapies: clinical evidence. Drug Resist Updat 2019;47:100646.
37. Martinez-Reyes I, Chandel NS. Mitochondrial TCA cycle metabolites control physiology and disease. Nat Commun 2020;11:102.
38. Liu Z, Butow RA. Mitochondrial retrograde signaling. Annu Rev Genet 2006;40: 159–85.
39. Yang D, Kim J. Mitochondrial retrograde signalling and metabolic alterations in the tumour microenvironment. Cells 2019;8:275.
40. Killian JK, Kim SY, Miettinen M, Smith C, Merino M, Tsokos M, et al. Succinate dehydrogenase mutation underlies global epigenomic divergence in gastrointestinal stromal tumor. Cancer Discov 2013;3:648–57.
41. Mason EF, Hornick JL. Succinate dehydrogenase deficiency is associated with decreased 5-hydroxymethylcytosine production in gastrointestinal stromal tumors: implications for mechanisms of tumorigenesis. Mod Pathol 2013;26: 1492–7.
42. Chakrabarty RP, Chandel NS. Mitochondria as signaling organelles control mammalian stem cell fate. Cell Stem Cell 2021;28:394–408.
43. Weinberg SE, Singer BD, Steinert EM, Martinez CA, Mehta MM, Martinez-Reyes I, et al. Mitochondrial complex III is essential for suppressive function of regulatory T cells. Nature 2019;565:495–9.
44. Diebold LP, Gil HJ, Gao P, Martinez CA, Weinberg SE, Chandel NS. Mitochondrial complex III is necessary for endothelial cell proliferation during angiogenesis. Nat Metab 2019;1:158–71.
45. Tsafou K, Katschnig AM, Radic-Sarikas B, Mutz CN, Iljin K, Schwentner R, et al. Identifying the druggable interactome of EWS-FLI1 reveals MCL-1–dependent differential sensitivities of Ewing sarcoma cells to apoptosis inducers. Oncotarget 2018;9:31018–31.
46. Marchetto A, Ohmura S, Orth MF, Knott MML, Colombo MV, Arrigoni C, et al. Oncogenic hijacking of a developmental transcription factor evokes vulnerability toward oxidative stress in Ewing sarcoma. Nat Commun 2020;11:2423.